

Electronic Supplementary Information (ESI)

Selective photoreduction of diluted CO₂ to CH₄ via topotactic transformation of mixed metal oxides derived from NiAlTi-LDH

Zhangyi Hu⁺, Da Ke⁺, Jiahao Min, Hongzhou Yang, Qingwen Meng, Fan Tian, Yu Chen, Xuyang Xiong^{}, Zuozuo Wu^{*} and Tengfei Zhou^{*}*

Z. Hu, D. Ke, J. Min, Q. Meng, Dr. X. Xiong, Prof. T. Zhou

Institutes of Physical Science and Information Technology, Key Laboratory of Structure and Functional Regulation of Hybrid Material (Ministry of Education), Anhui University, Hefei, Anhui, 230601, China

Email: xuyang@ahu.edu.cn; tengfeiz@ahu.edu.cn

Dr. H. Yang

Anhui Provincial Key Laboratory of Magnetic Functional Materials and Devices, School of Materials Science and Engineering, Anhui University, Hefei, Anhui, 230601, China.

Prof. F. Tian

School of Chemistry and Environmental Engineering, Wuhan Institute of Technology, Wuhan, Hubei, 430205, China.

Dr. Y. Chen

Shanghai Synchrotron Radiation Facility, Shanghai Advanced Research Institute, Chinese Academy of Sciences, Shanghai, 201204, China

Dr. Z. Wu

School of Materials Science and Engineering, Zhejiang University, Hangzhou, Zhejiang, 310027, China. E-mail: zuozuowu@zju.edu.cn

Keywords: photocatalysis; diluted CO₂-to-CH₄ conversion; Ti³⁺ sites; -OH functionalized; LDH topology transformation;

Materials:

Nickel nitrate hexahydrate ($\text{Ni}(\text{NO}_3)_2 \cdot 6\text{H}_2\text{O}$), aluminum nitrate nonahydrate ($\text{Al}(\text{NO}_3)_3 \cdot 9\text{H}_2\text{O}$), tetra-n-butyl titanate ($\text{Ti}(\text{OC}_4\text{H}_9)_4$), sodium carbonate (Na_2CO_3), sodium hydroxide (NaOH), acetic acid (CH_3COOH), ethylene glycol ($\text{C}_2\text{H}_6\text{O}_2$). All these chemicals were of analytical grade and used without further purification. Doubly distilled water was used in all experiments.

Preparation of NiO, NAM₃₀₀, TiO₂, Al₂O₃, Ti³⁺-OH/NAM₃₀₀ and Ti³⁺/NAM₅₀₀:

NiO: 25 mmol $\text{Ni}(\text{NO}_3)_2 \cdot 6\text{H}_2\text{O}$ was added into 40 mL deionized water under continuous stirring to form a green solution. The pH was adjusted to around 10 using a mixed solution of Na_2CO_3 and NaOH . The solution obtained was then continuously stirred at 50 °C for 2 h, and then oil bath treated at 90 °C for 12 h. The solid obtained was washed with H_2O for five times to remove surface residual ions. Finally, it was transferred to a muffle furnace for calcination at 300°C for 2 hours.

NAM₃₀₀: 25 mmol $\text{Ni}(\text{NO}_3)_2 \cdot 6\text{H}_2\text{O}$, 8.4 mmol $\text{Al}(\text{NO}_3)_3 \cdot 9\text{H}_2\text{O}$ were added into 40 mL deionized water under continuous stirring to form a green solution. Then, the remaining steps are the same as those used in the synthesis of NiO. The meaning of “NAM” is “NiAl Mixed Metal Oxides”.

TiO₂: 5 mmol $\text{Ti}(\text{OC}_4\text{H}_9)_4$ was added into 20 mL mixture of ethylene glycol and oxalic acid solution under continuous stirring to form a solution. The solution obtained was then continuously stirred at 50 °C for 2 h, and then oil bath treated at 90 °C for 12 h. The solid obtained was washed with H_2O for five times to remove surface residual ions. Finally, it was transferred to a muffle furnace for calcination at 300°C for 2 hours.

Al₂O₃: 8.4 mmol $\text{Al}(\text{NO}_3)_3 \cdot 9\text{H}_2\text{O}$ were added into 40 mL deionized water under continuous stirring to form a solution. Then, the remaining steps are the same as those used in the synthesis of NiO.

Ti³⁺-OH/NAM₃₀₀ and Ti³⁺/NAM₅₀₀: 25 mmol $\text{Ni}(\text{NO}_3)_2 \cdot 6\text{H}_2\text{O}$, 3.4 mmol $\text{Al}(\text{NO}_3)_3 \cdot 9\text{H}_2\text{O}$ were added into 40 mL deionized water under continuous stirring to form a green solution. 5 mmol $\text{Ti}(\text{OC}_4\text{H}_9)_4$ was added into 20 mL mixture of ethylene glycol and oxalic acid solution under continuous stirring to form a transparent solution. Then, the transparent solution was slowly added to the green solution. The pH was adjusted to around 10 using a mixed solution of Na_2CO_3 and NaOH . The solution obtained was then continuously stirred at 50 °C for 2 h, and then oil bath treated at 90 °C for 12 h. The solid obtained was washed with H_2O for five times to remove surface residual ions. Finally, it was transferred to a muffle furnace for calcination at 300°C and

500°C for 2 hours.

Characterization:

Powder X-ray diffraction (XRD) patterns for the various catalysts and photocatalysts were collected on a Germany Bruker D2 PHASER X-ray diffractometer equipped with a Cu K α radiation source ($\lambda = 0.15418$ nm). X-ray photoelectron spectroscopy (XPS) data were collected on an ESCALAB 250 X-ray photoelectron spectrometer, using non-monochromatic Mg-K α X-ray as the excitation source, and all binding energy of samples were corrected by referencing the C 1s peak to 284.8 eV of adventitious hydrocarbons. Transmission electron microscopy (TEM) and high-resolution TEM (HRTEM) images were collected on a FEI Tecnai F20 microscope operating at an accelerating voltage of 200 kV. Samples were dispersed on hydrophilic carbon films for the analyses. The instrument was also equipped with EDX elemental mapping on X-Twin. The electron paramagnetic resonance (EPR) test was conducted on Bruker A300. UV-vis diffuse reflectance spectra were collected on Varian Cary 100 Scan UV-Vis system with BaSO₄ as the reflectance standard. Ni, Ti K-edge X-ray absorption fine structure (XAFS) measurements were performed on the 111 beamline of Shanghai Synchrotron Radiation Facility (SSRF). All the measurements were performed at room temperature and atmospheric pressure with a solid sample.

Photocatalytic CO₂ reduction tests:

Typically, CO₂ photoreduction experiment was carried out in a customized stainless steel-lined reactor. 5 mg of the catalyst was uniformly dispersed on a glass fiber filter membrane, with 20 μ L of deionized water added as the proton source. Then, gas was introduced into the sealed container with pure CO₂ (99.99%) or diluted CO₂ (90%Ar +10% CO₂) for 20 min with 300 W Xe lamp as the light source. During light irradiation, 1 mL of gaseous mixture was collected from the reactor at regular time intervals. The products were analyzed by China Education Au-light GC-7920 chromatography, which was equipped with both flame ionization detector (FID) and thermal conductivity detector (TCD). The Apparent quantum yield (AQY) was calculated by using 350 nm light filter with light intensity about 0.1 W/cm² through Eq:

$$AQY = \frac{Ne}{Np} \times 100\% = \frac{(\nu \times N_A \times K) \times (h \times c)}{(\varphi \times \lambda)} \times 100\%$$

Where Ne is the total number of electrons transferred by the reaction, Np is the incident photon

number, v is reaction rate (mol s^{-1}), N_A is Avogadro's constant ($6.02 \times 10^{23} \text{ mol}^{-1}$), K is the number of electrons transferred by the reaction, h is Planck's constant, c is the speed of light, ϕ is the light intensity, λ is the wavelength.

Electrochemical tests:

Electrochemical measurements were performed on a DH 7000C electrochemical workstation equipped with a three-electrode cell. For electrochemical impedance spectroscopy (EIS) measurements, the working electrode was a glassy carbon electrode coated with catalyst, the counter electrode was a platinum foil, and the reference electrode was a saturated Ag/AgCl electrode. Na_2SO_4 (1 mol L^{-1} , 50 mL) served as the electrolyte with the EIS data collected over the frequency range 0.01-10⁵ Hz.

In-Situ FTIR Measurement: In situ FT-IR spectra was acquired at the Infrared Spectroscopy and Microscopic Imaging End station at the BL01B beamline of the National Synchrotron Radiation Laboratory (NSRL, Hefei, Anhui province). And the spectrum was recorded on a FT-IR spectrometer (German Bruker IFS66v/S). 30 mg of catalyst, a mixture of high-purity (99.99%) CO_2 and deionized water were poured into the reactor. The system was first maintained under dark conditions for 30 minutes to establish adsorption-desorption equilibrium. Then, the reactor was irradiated using a 300 W xenon lamp with 10-minute as the time interval to record the produced gas signals.

DFT calculation details:

Spin-polarized DFT calculations were performed using the Atomic-orbital Based Ab-initio Computation at USTC (abacus 3.8). The exchange–correlation interactions were treated with the Perdew–Burke–Ernzerhof (PBE) functional in the generalized gradient approximation (GGA). The projection augmented wave (PAW) potential method was used to describe the interaction between atomic nuclei and electrons. The empirical correction method in the Grimme scheme (DFT + D3) was used to describe the van der Waals (vdW) interactions of reactants or intermediates and catalysts.

A $3 \times 3 \times 2$ TiO_2 supercell was used as the initial model. A kinetic energy cutoff of 450 eV was set for the plane-wave basis. van der Waals (vdW) corrections were included by adopting the zero damping DFT-D3 dispersion model developed by Grimme et al. A 15 Å-thick vacuum layer was added to the z-direction to separate slabs from their periodic images. The Monk horst–Pack scheme was adopted to sample the Brillouin region with a $(3 \times 3 \times 2)$, k-point mesh grid for supercell structure optimization. The convergence thresholds of energy and force were set to 10^{-6} eV and 0.03 eV \AA^{-1} , respectively. The free energy correction of the adsorbed molecules was processed using a vaspkit

script. The free energy parameter has been widely used to evaluate the catalytic performance of electrocatalysts and it was obtained by calculating the hydrogen electrode model (CHE).

Equation for the change in Gibbs free energy of CO₂RR:

$$\Delta G = \Delta E + \Delta ZPE - T\Delta S$$

Where ΔE represents the change of total energy between the reactants and the products derived by the DFT technique, ΔZPE is the zero-point energy correction via frequency analysis, and ΔS is the change of entropy during each elementary step at a finite temperature of 298.15 K.

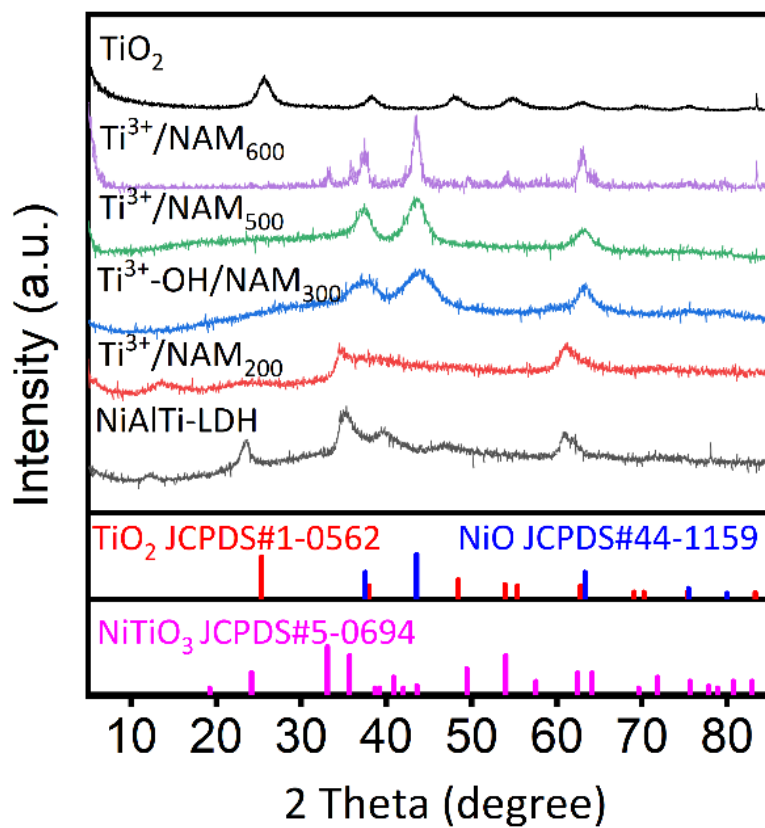


Fig. S1 XRD pattern of NiAlTi-LDH, TiO_2 and $\text{Ti}^{3+}/\text{NAM}_x$.

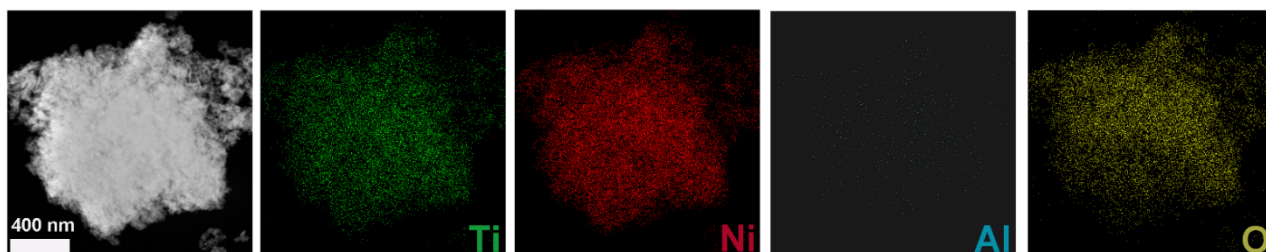


Fig. S2 EDS mapping of $\text{Ti}^{3+}\text{-OH}/\text{NAM}_{300}$.

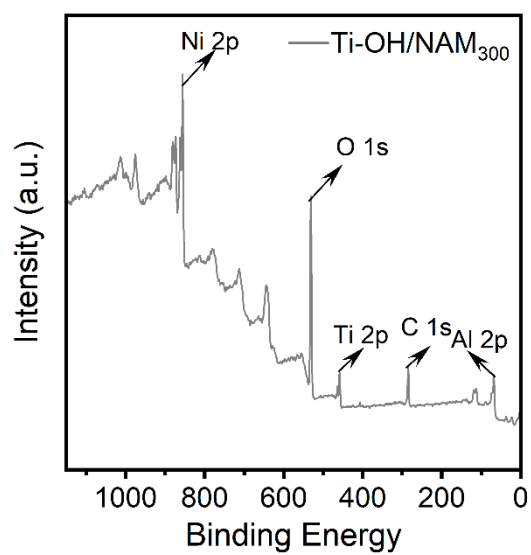


Fig. S3 Full-Scan XPS spectra of Ti^{3+} -OH/NAM₃₀₀.

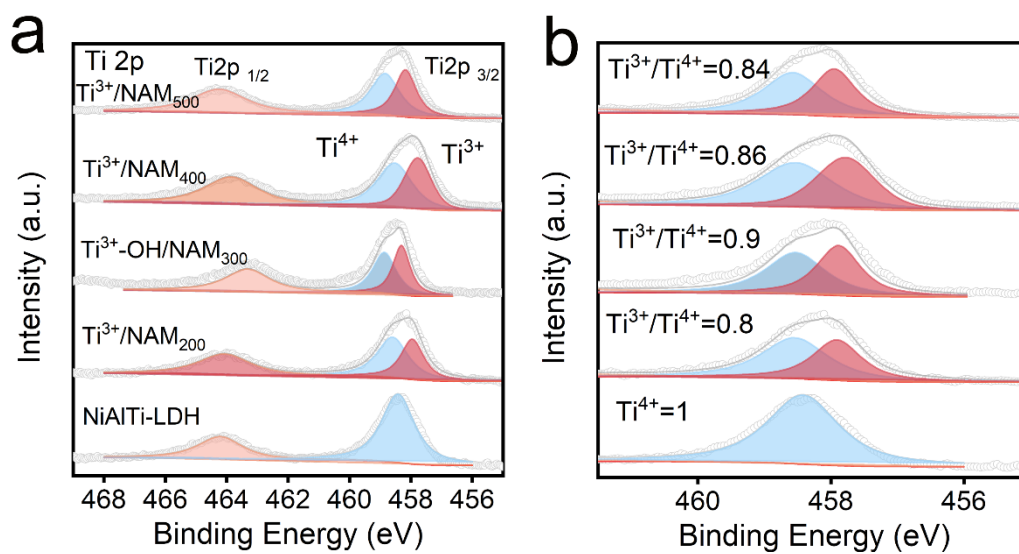


Fig. S4 XPS spectra of Ti2p orbitals collected from NiAlTi-LDH and Ti^{3+} /NAM_x.

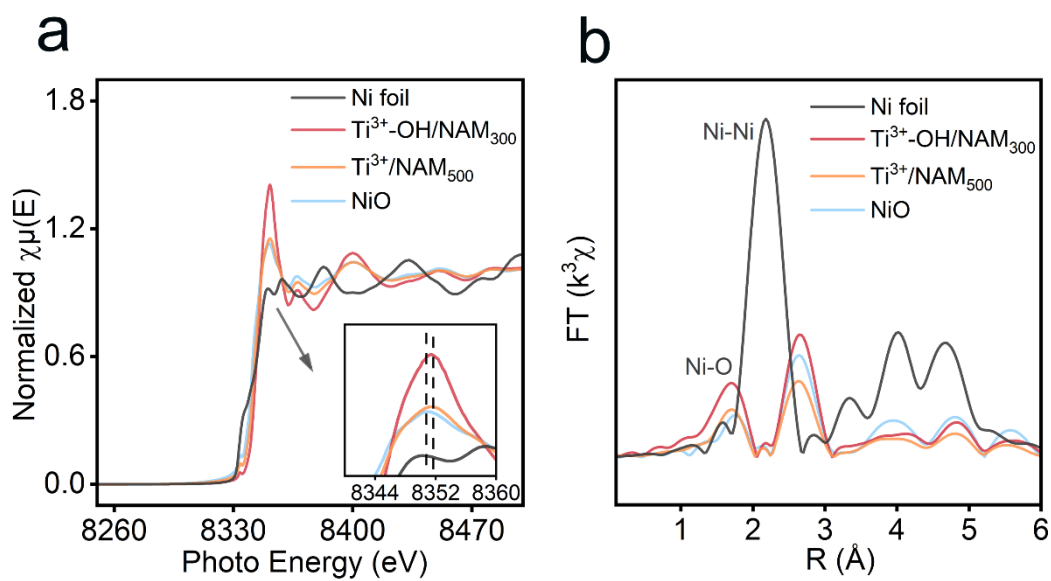


Fig. S5 (a) The normalized Ni K-edge XANES and (b) FT-EXAFS XANES spectra for NiO, Ni foil, $\text{Ti}^{3+}\text{-OH/NAM}_{300}$, and $\text{Ti}^{3+}\text{/NAM}_{500}$.

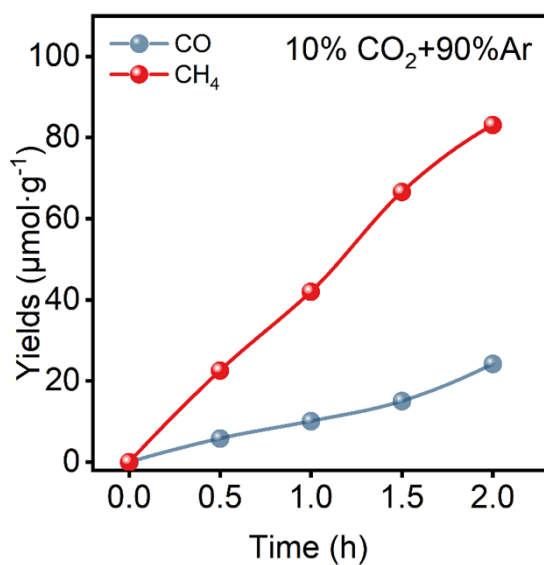


Fig. S6 The time-dependent curves of CH_4 and CO evolution yields by $\text{Ti}^{3+}\text{-OH/NAM}_{300}$.

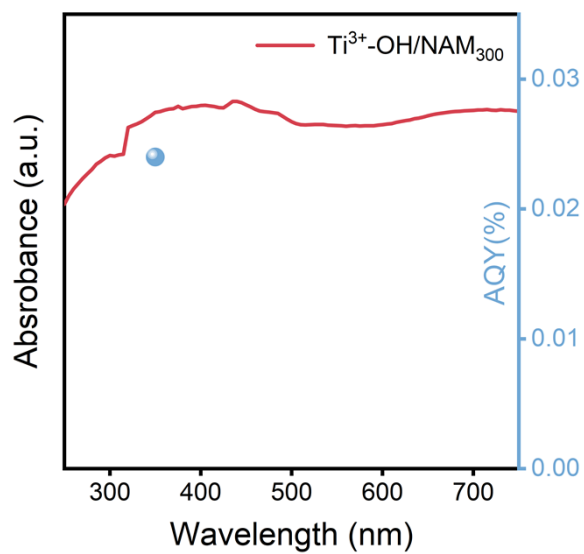


Fig. S7 Apparent quantum yield of $\text{Ti}^{3+}\text{-OH/NAM}_{300}$

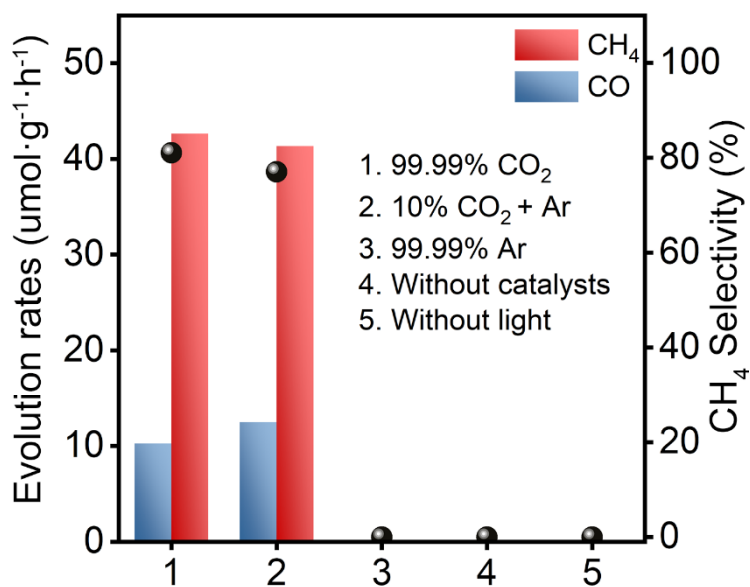


Fig. S8 The photocatalytic CO_2 reduction performance under different conditions.

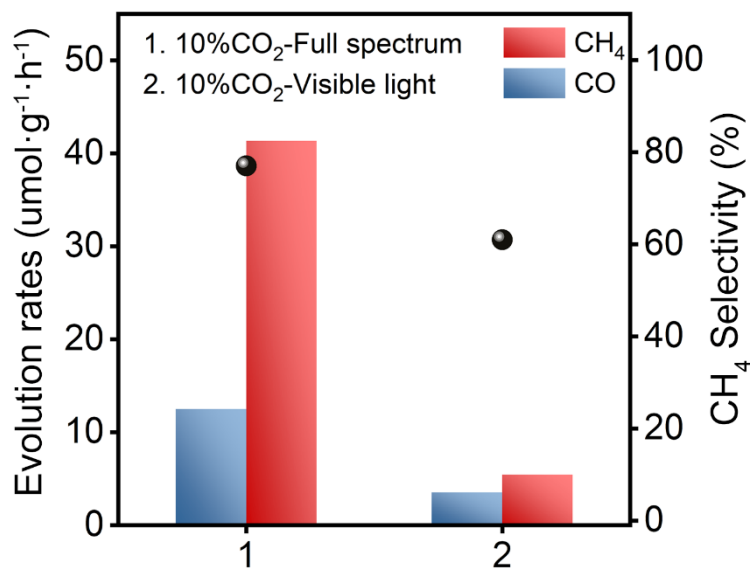


Fig.S9 The photocatalytic CO₂ reduction performance under visible light of Ti³⁺-OH/NAM₃₀₀.

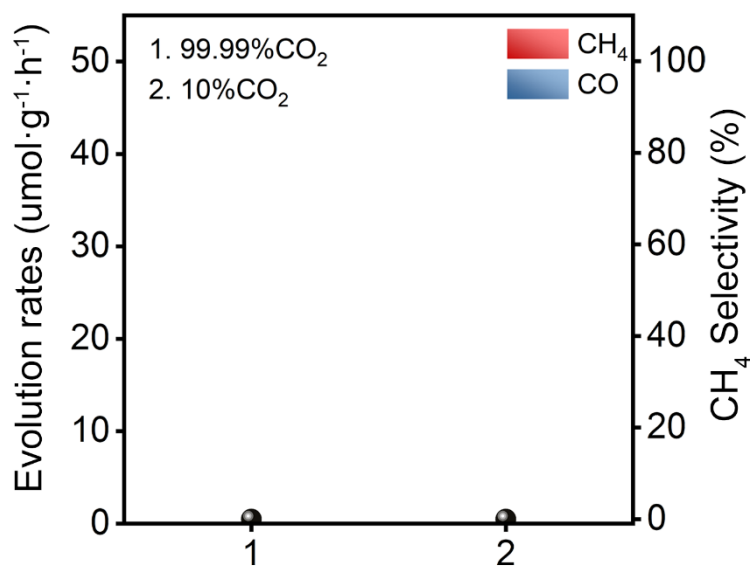


Fig.S10 The photocatalytic CO₂ reduction performance of Al₂O₃

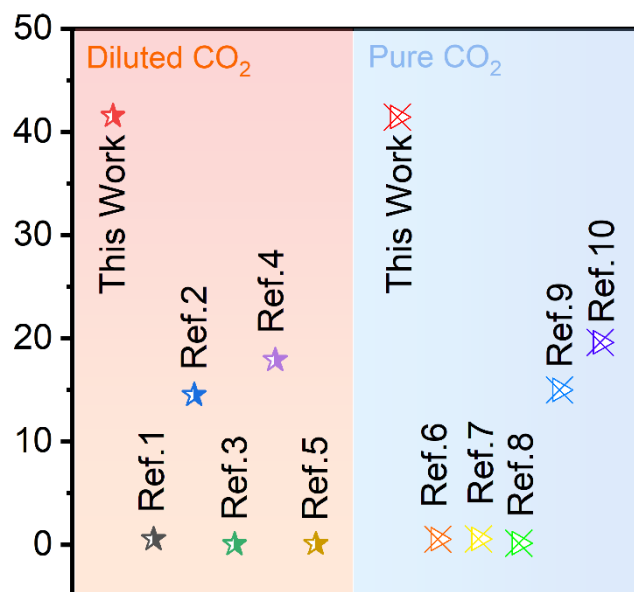
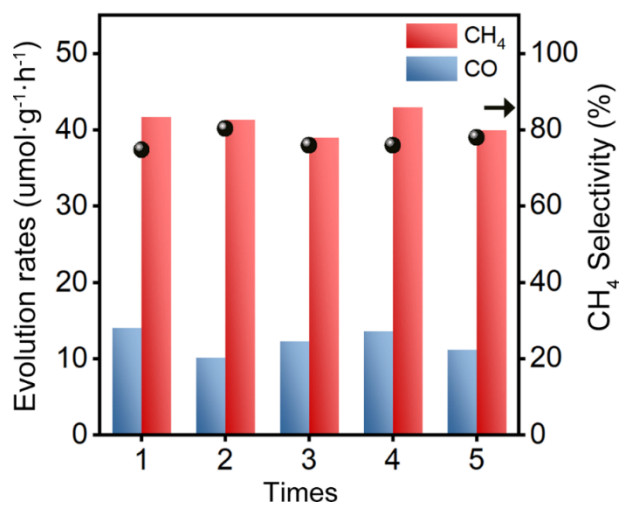


Fig. S11 Summary of photocatalytic CO₂ to CH₄ activity involving Ti-based catalysts (Red and blue backgrounds represent diluted and pure CO₂ atmospheres respectively).

Table S1. The CO₂-to-CH₄ conversion activities of various Ti-based photocatalysts.

CO ₂ Atmosphere	Catalyst	CH ₄ Evolution rates($\mu\text{mol}\cdot\text{g}^{-1}\cdot\text{h}^{-1}$)	Year	light conditions	CH ₄ selectivity	AQY
99.99%	TiO ₂ / CdSe ⁶	0.525	2024	full	100%	/
99.99%	Ti ³⁺ self-doped TiO ₂ ⁷	0.557	2024	UV	100%	/
99.999%	Cu ₂ O clusters/TiO ₂ ⁸	0.15	2022	UV-VIS	72%	/
99.99%	CeO ₂ /ATiO ₂ HoMSs 9	15	2022	full	100%	/
99.99%	Pd ₇ Cu ₁ -TiO ₂ ¹⁰	19.6	2017	full	96%	/
10% CO ₂	Pt-TiO ₂ ¹	0.53	2023	full	94.71%	/
10% CO ₂	Ag-TiO ₂ ²	14.5	2022	full	70.8%	/
1000 ppm	NGO-RT ³	0.036	2021	visible	100%	/
2% CO ₂	TiO ₂ /UiO-66 ⁴	17.9	2020	full	90.4%	/
1000 ppm	RT-Cu ₂ O ⁵	0.077	2020	full	/	/

**Fig. S12** CO and CH₄ formation rates of Ti³⁺-OH/NAM₃₀₀ sample for five cycles.

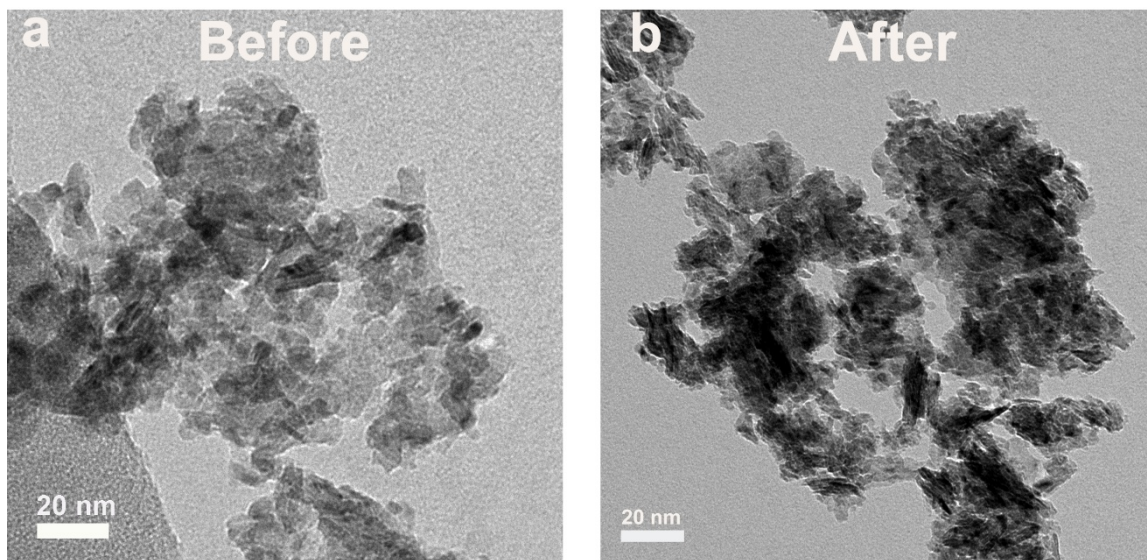


Fig. S13 TEM image of $\text{Ti}^{3+}\text{-OH/NAM}_{300}$ before and after photocatalytic CO_2 reduction

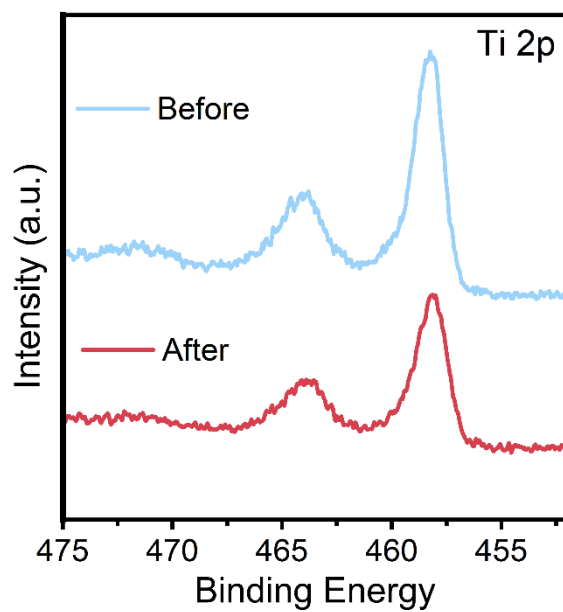


Fig. S14 XPS patterns of $\text{Ti}^{3+}\text{-OH/NAM}_{300}$ before and after photocatalytic CO_2 reduction.

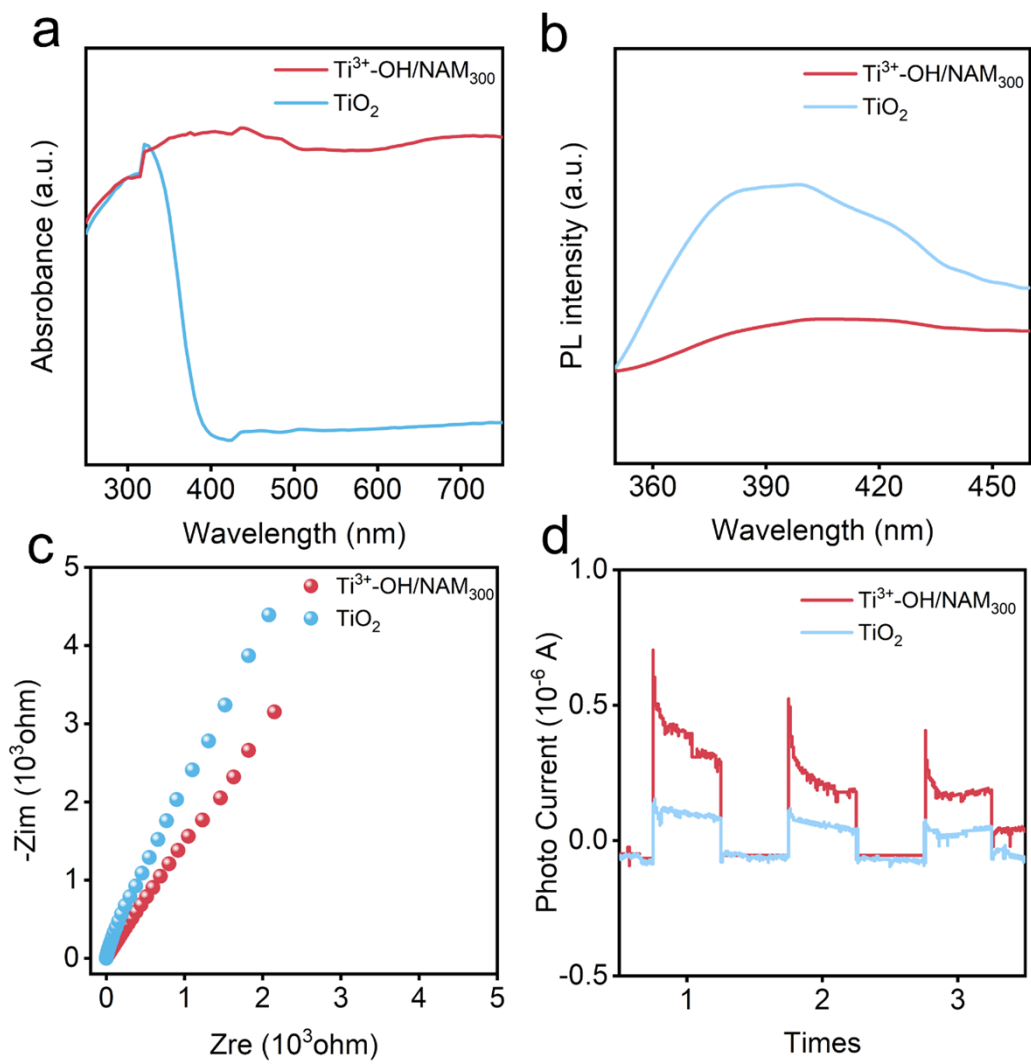


Fig. S15 (a) Diffuse reflectance spectra for $\text{Ti}^{3+}\text{-OH/NAM}_{300}$ and TiO_2 ; (b, c, d) steady-state PL spectra, EIS and photocurrent patterns for $\text{Ti}^{3+}\text{-OH/NAM}_{300}$ and TiO_2 .

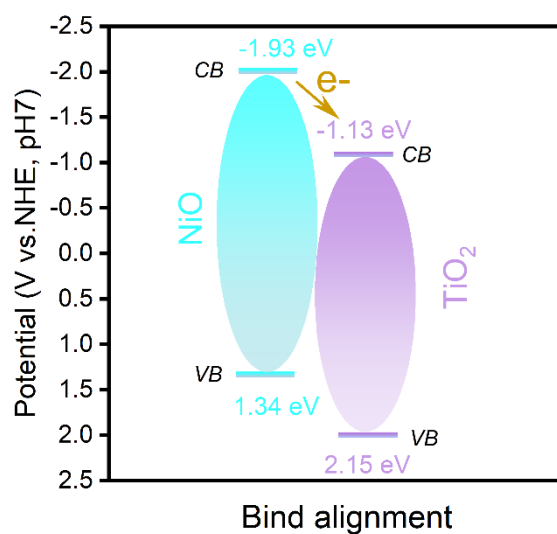


Fig. S16 The band alignments of NiO and TiO₂.

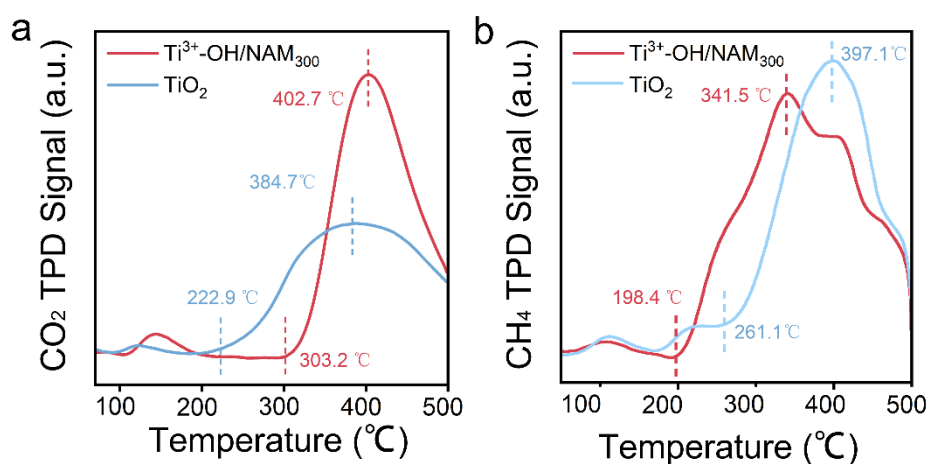


Fig. S17 (a)CO₂ and (b)CH₄ TPD profiles of Ti³⁺-OH/NAM₃₀₀ and TiO₂

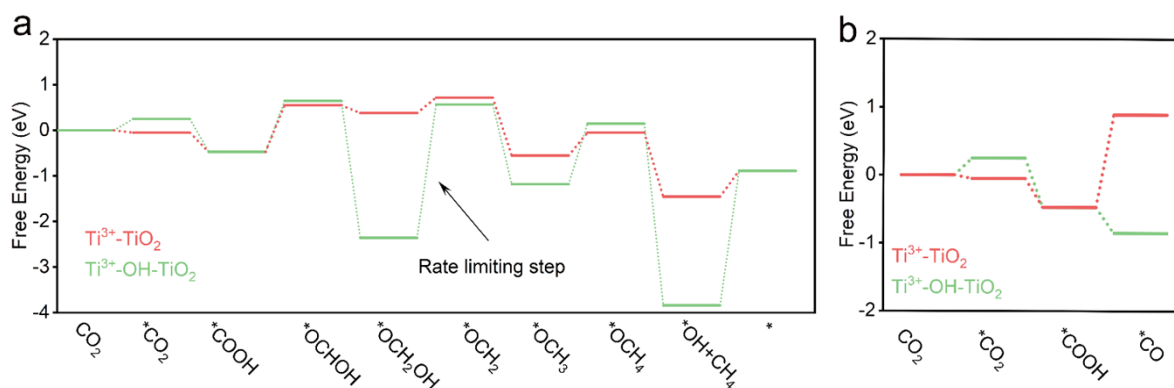


Fig. S18 Free energy profiles for the elementary steps of CO₂-to-CH₄ and CO₂-to-CO pathways over Ti³⁺-TiO₂ and the Ti³⁺-OH-TiO₂ model.

Reference:

- [1] Y. Liu, S. Kang, T. Li, Z. Hu, Y. Ren, Z. Pan, X. Fu, L. Wang, S. Feng, J. Luo, L. Feng, W. Lu, *Phys. Chem. Chem. Phys.*, 2022, **24**, 15389–15396.
- [2] H. Huang, R. Shi, Z. Li, J. Zhao, C. Su, T. Zhang, *Angew. Chem. Int. Ed.*, 2022, **61**, e202200802.
- [3] C. B. Hiragond, J. Lee, H. Kim, J. Jung, C. H. Cho, S. In, *Chem. Eng. J.*, 2021, **416**, 127978.
- [4] Y. Ma, Q. Tang, W. Sun, Z. Yao, W. Zhu, T. Li, J. Wang, *Appl. Catal. B*, 2020, **270**, 118856.
- [5] S. Ali, J. Lee, H. Kim, Y. Hwang, A. Razzaq, J. Jung, C. Cho, S. In, *Appl. Catal. B*, 2020, **279**, 119344.
- [6] N. Powar, S. Kim, J. Lee, E. Gong, C. Hiragond, D. Kim, T. Zhang M. Kim, S. In, *Appl. Catal. B*, 2024, **352**, 124006.
- [7] R. Ricka, A. Wanag, E. K. Nejman, D. Moszyński, M. Edelmannová, M. Reli, Z. Baďura, G. Zoppellaro, R. Zbořil, A. W. Morawski, K. Kočí, *J. CO₂ Util.*, 2024, **80**, 102701.
- [8] Z. Wang, Y. Shi, C. Liu, Y. Kang, L. Wu, *Appl. Catal. B*, 2022, **301**, 120803.
- [9] Y. Wei, F. You, D. Zhao, J. Wan, L. Gu, D. Wang, *Angew. Chem. Int. Ed.*, 2022, **61**, e202212049.
- [10] R. Long, Y. Li, Y. Liu, S. Chen, X. Zheng, C. Gao, C. He, N. Chen, Z. Qi, L. Song, O. Jiang, J. Zhu, Y. Xiong, *J. Am. Chem. Soc.*, 2017, **139**, 4486-4492.